TRAPPED-ION QCCD

WOLFGANG PAUL FACTS

Photo from the Nobel Foundation archive.

Wolfgang Paul
Nobel Prize in Physics 1989

Born: 10 August 1913, Lorenzkirch, Germany

Died: 7 December 1993, Bonn, Germany

Affiliation at the time of the award: University of Bonn, Bonn, Germany

Prize motivation: “for the development of the ion trap technique”

Prize share: 1/4

https://www.nobelprize.org/prizes/physics/1989/paul/facts/

NOBEL PRIZE 1989:

WORK

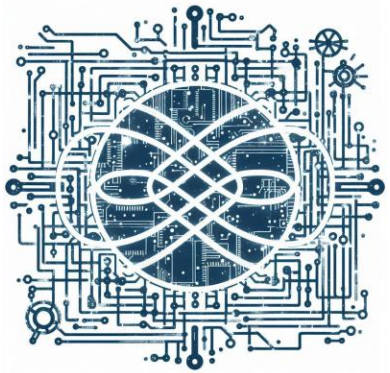

The properties of atoms are determined by laws of quantum mechanics that say they can have only fixed energy levels and that electromagnetic radiation with certain frequencies is emitted or absorbed when there are transitions among different energy levels. Opportunities to study the properties and spectrums of atoms are improved if individual atoms can be isolated under constant conditions for longer periods. In the 1950s Wolfgang Paul developed a method for using electrical currents and electromagnetic fields to capture charged atoms—ions—in a trap.

https://www.nobelprize.org/prizes/physics/1989/paul/facts/

DEMONSTRATION OF THE TRAPPED-ION QUANTUM-CCD COMPUTER ARCHITECTURE.

(PINO ET AL., 2020)

FIG. 1.

The programmable QCCD quantum computing system. (a) Right, a picture of the trap. Left, the information ow from the user to the trapped ion qubits. From top to bottom, we illustrate: user, cloud, internal tasking, machine control system, FPGA. The circuits are processed by a compiler to generate control signals (purple) sent to both the trapand the optoelectronic devices controlling the laser beams. An imaging system and PMT array collect and count scattered photons, and the results (green) are sent back to the software stack and user, or processed for real-time decision making. (b) A schematic of the trap: RF electrodes (green), loading hole (black), load zone (pink), extended gate zones (orange), gate zones (blue), and auxiliary zones (yellow) for qubit storage. In this work, only the gate zones with grey circles are used. (c) A general quantum circuit: ions already sharing a gate zone are gated, then spatially isolated for SQ gates, then the second and third ions are swapped for the nal TQ gates. While not shown, readout, TQ gates, and SQ gates can all be performed in parallel across diferent zones. (p.2).

A LINEAR TRACK

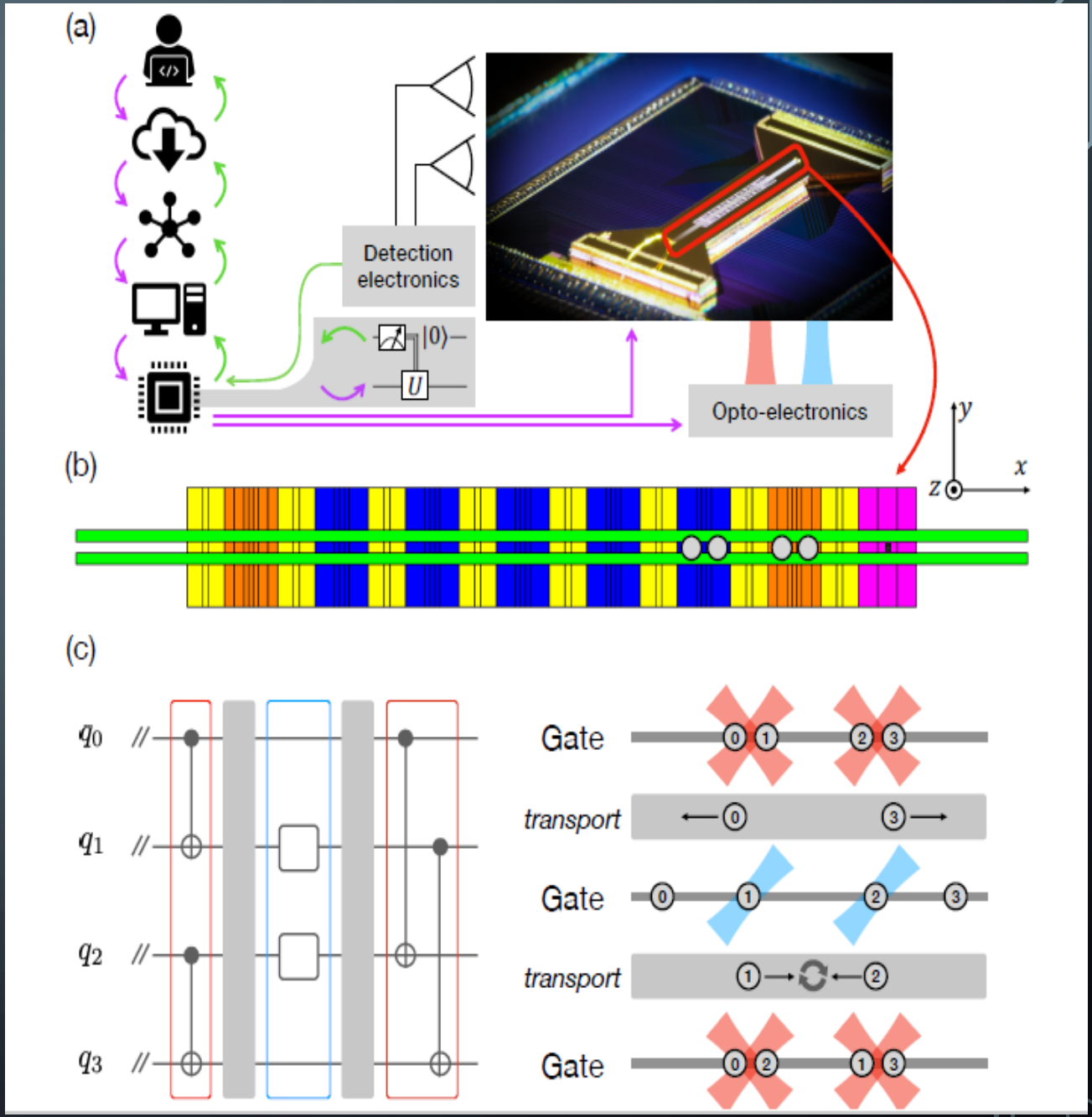

Pino et. Al., 2021, p.2, https://doi.org/10.48550/arXiv.2003.01293

A RACE-TRACK TRAPPED-ION QUANTUM PROCESSOR.

(MOSES ET AL., 2023)

FIG. 1.

Picture of the H2 surface ion trap microchip. The image has been modified to enhance visibility of the trap features. The trap sits in the isthmus in the center of the trap die. The long axis of the trap is 6.58 mm (from the edge of the dc electrodes on either side), and the isthmus width is 2.02 mm. (Moses et al., 2023, p. 1)

https://arxiv.org/abs/2305.03828

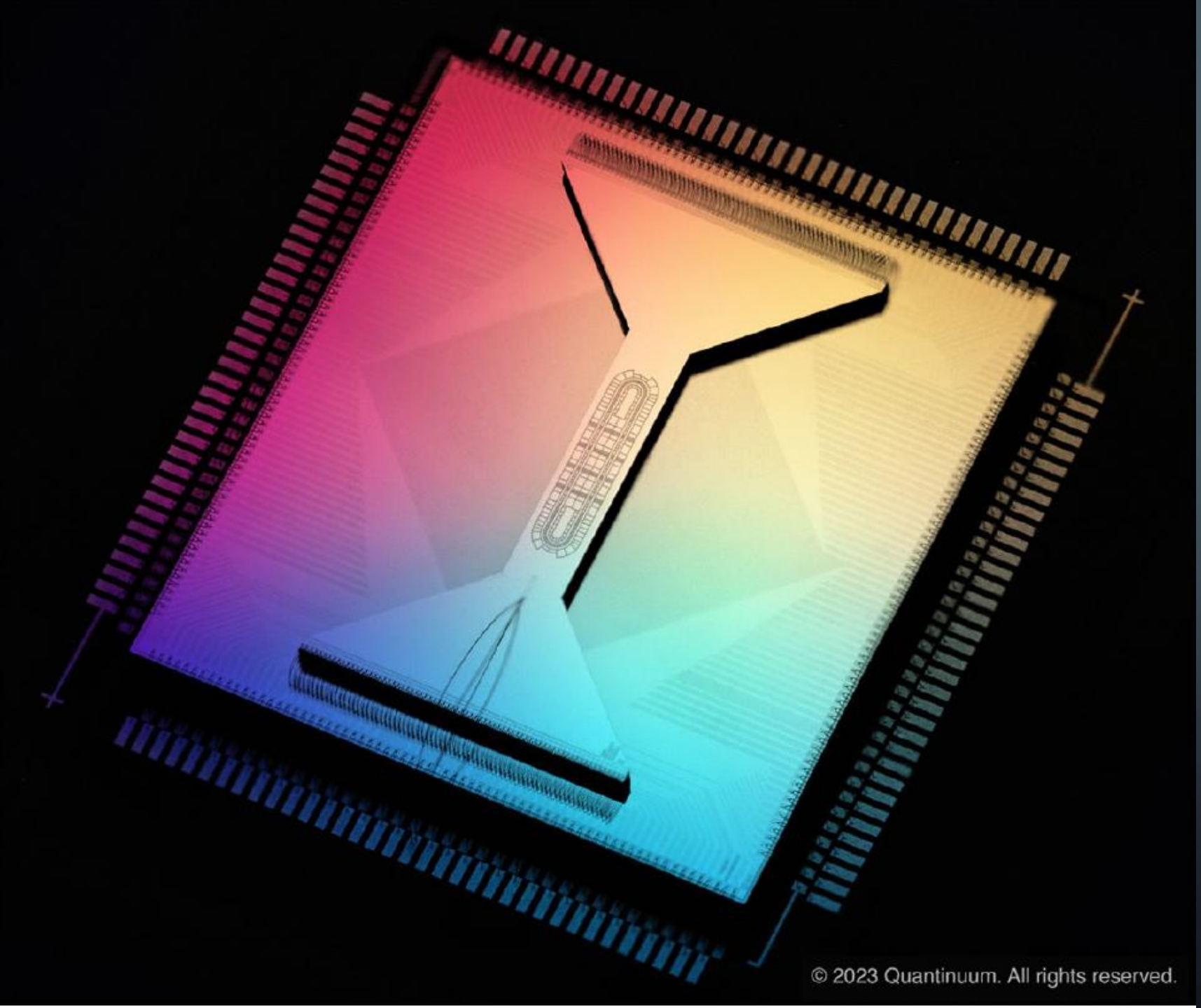

We can see the race track in the center.

FIG. 2.

Overview of the H2 trap including upgrades in trap design and gating operations. (a) 2D MOT producing a collimated beam of atoms, allowing for higher neutral atom density and faster loading than an effusive oven. (b) The abc tiling of electrodes for conveyor belt transport. (c) rf tunnels to implement inner and outer rf electrodes. Ions are trapped 70 µm away fromthe trap surface. (d) Colored topmetal layer of the H2 trap. Green curved zones are conveyor belt regions for ion storage. The bottom blue zones are DG01–DG04 (from left to right), which are used for quantum operations. The top blue zones are UG01–UG04 gate zones (from right to left), which are used for sorting but not quantum operations. Darker gray loops are rf electrodes. Yellow circles represent qubits that are gated while red circles represent qubits sitting in storage during gates (note that 138Baþ ions are omitted for simplicity). Yellow arrows indicate the Doppler sheet beam direction while blue arrows indicate the Doppler repump sheet beam direction. (e) Ion configuration and beam direction for 2Q gates. Large orange circles represent 171Ybþ while smaller purple circles represent 138Baþ. (f) Ion configuration and beam directions for 1Q gates on the left 171Ybþ. (g) Ion configuration and beam directions for state preparation and measurement (SPAM) operations on the left 171Ybþ with micromotion hiding on the right 171Ybþ [31]. (h) Storage ion configuration in the conveyor belt region. (p. 3)

[Moses et al., 2023: https://arxiv.org/abs/2305.03828

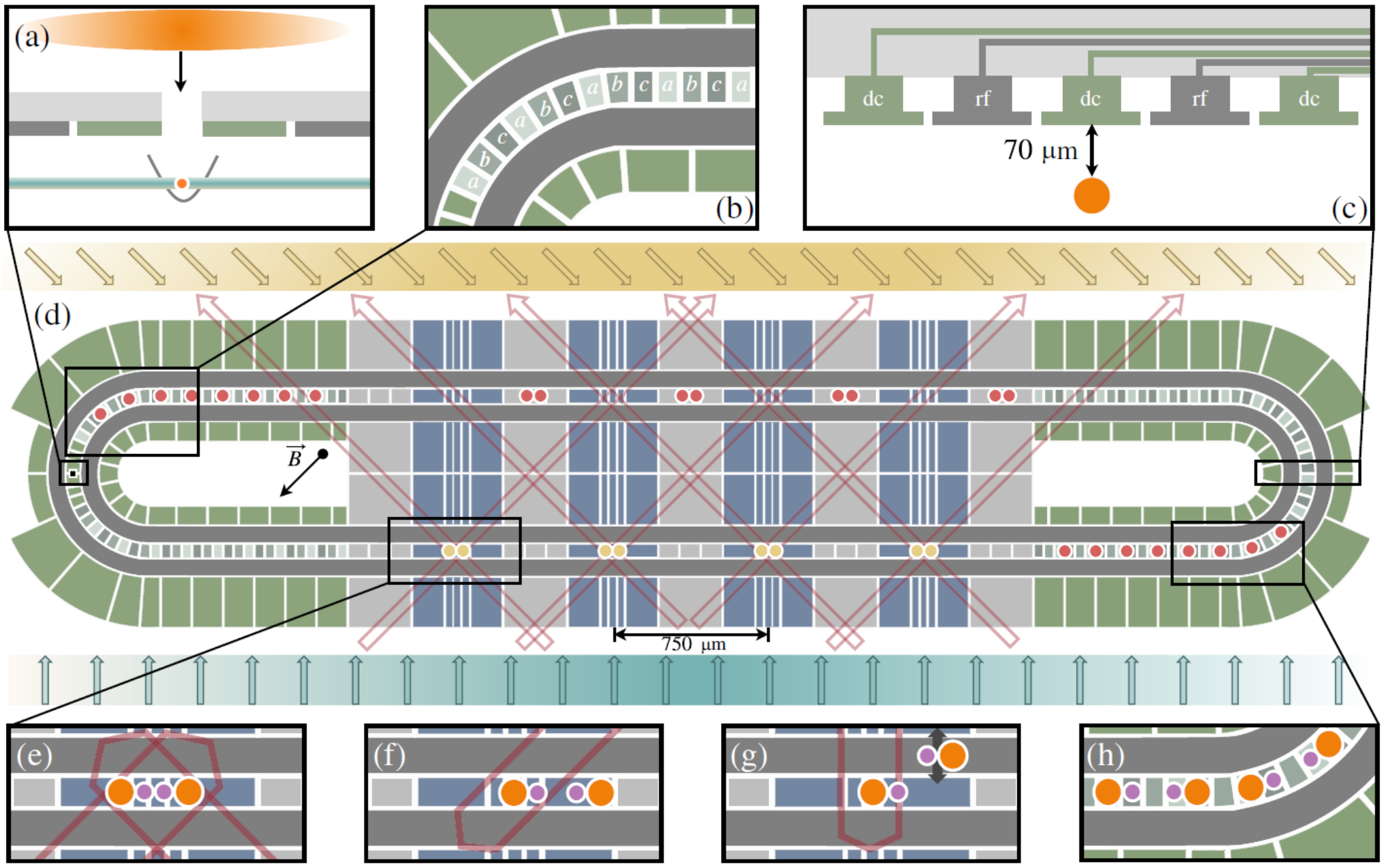
(a)
(b)
a b c a b c a b c a
(c)
dc
rf
dc
rf
dc
70 μm
(d)
$\vec{B}$
750 μm
(e)
(f)
(g)
(h)

THE COMPUTATIONAL POWER OF RANDOM QUANTUM CIRCUITS IN ARBITRARY GEOMETRIES

(DECROSS ET AL., 2024)

QUANTUM COUPED-CHARGE DEVICE & QUANTUM RANDOM CIRCUITS

This study guide explores the computational power of quantum random circuits (RCS) in various geometries, focusing on the architecture of Quantinuum's quantum computer H2. The study analyzes the complexity of the classic RCS simulation, highlighting the influence of circuit geometry on the difficulty of the simulation. Complexity density is explored as a metric to quantify the difficulty of the simulation, comparing random geometries with 2D geometries.

The paper also presents experimental results of RCS execution in H2, including fidelity estimates using mirror benchmarking techniques and linear cross-entropy. The details of the implementation are discussed, including gate benchmarking and handling memory errors during ion transport. In addition, approximate simulation methods, such as the density matrix renormalization group (DMRG), are explored, evaluating their ability to simulate RCS with achievable fidelities on current hardware.

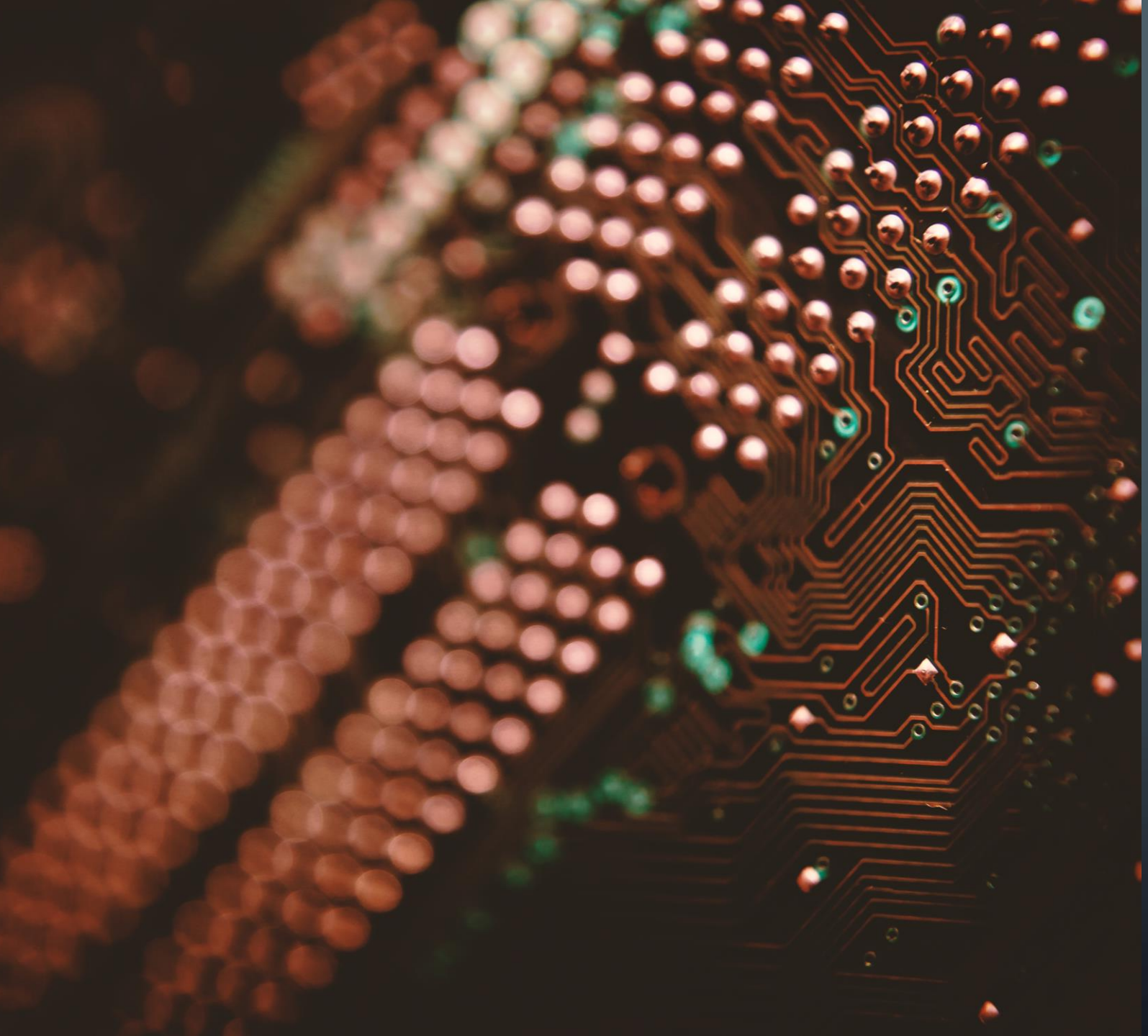

DESIDERABLE PHYSICAL PROPIERTIES

- MORE QUBITS
- LOWER PHYSICAL ERROR RATES
- HIGER CONNECTIVITY
- FASTER CLOCK SPEED

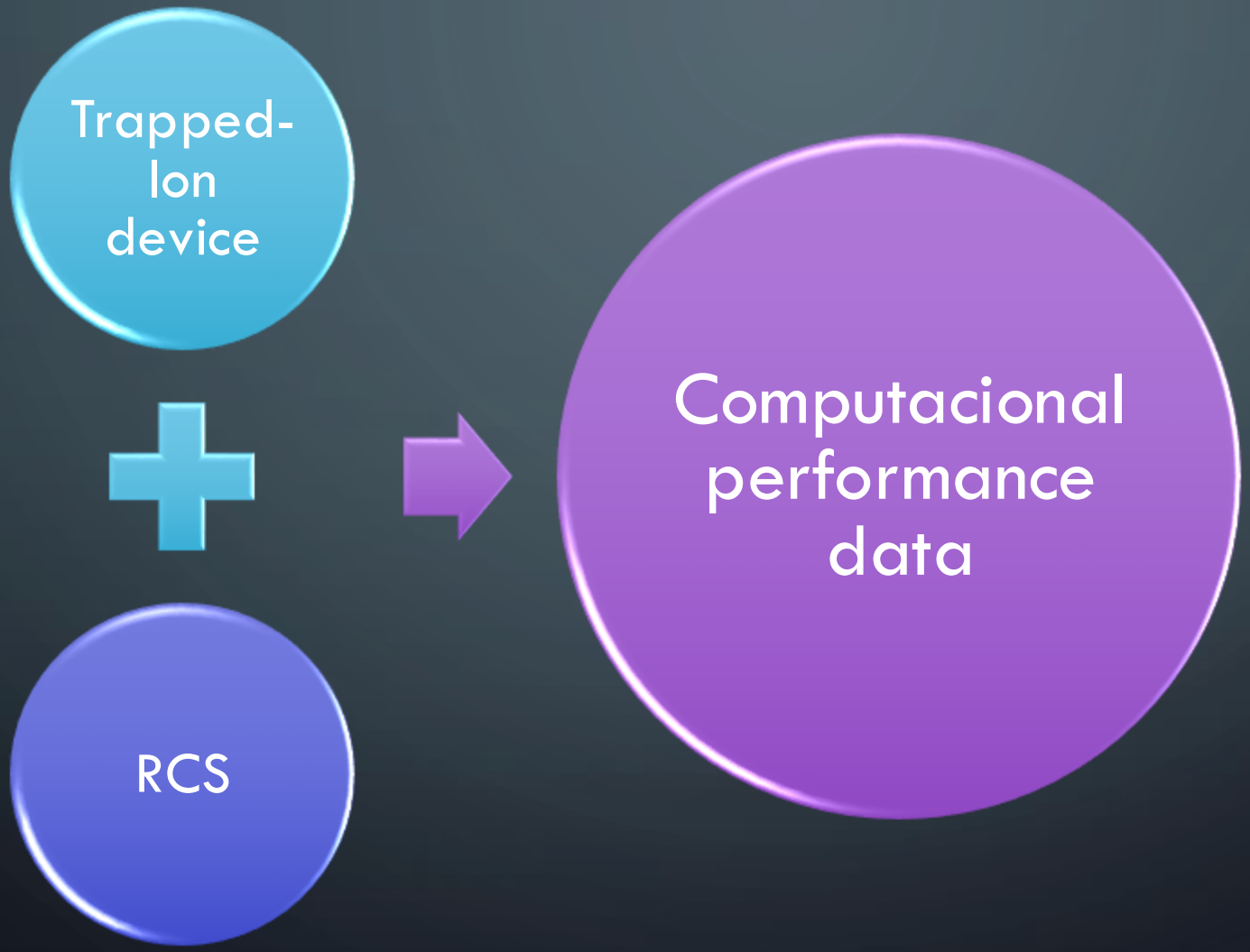
Trapped-Ion device
RCS
Computacional performance data

FIG. 1.

Demonstration of how a densely-gated circuit (N/2 2Q gates per layer) with arbitrary connectivity is executed on the H2 quantum computer. (a) The first layer is executed by assigning each qubit to a unique 171Yb+ ion (colored disk) such that gated qubits are co-located; each ion is labeled by a unique color, and the black lines connecting neighbors indicate that the associated qubits will be gated. Since H2 is currently configured with 4 active gate zones, the two-qubit (2Q) gates are executed in 7 batches of 4 parallel gates. (b) The first batch of four gates [highlighted in magenta in (a)] are executed in parallel in the bottom row of gate zones, and qubits are then shuffled around the trap in a "rolodex" fashion until all gates (including 1Q gates) in the first layer have been applied. (c) The next layer of gates can act on arbitrary pairs. (d) An automated compilation step decides where to locate qubits in the trap (placement) and how to get them there (routing), resulting in a new assignment of qubit positions that ensures all pairs of qubits to be gated in this layer are once again co-located. Given the placement determined in (d), sequences of voltages are applied to the trap electrodes that, via a combination of the split/combine, shift, and swap operations shown in (e) achieve the desired ion placement for this layer of gates shown in (f). The gates can once again be executed in a rolodex fashion, and this entire process is repeated until all layers of gates have been applied. Note that additional coolant ions are omitted in these illustrations; as described in Ref. [5, 6] each 171Yb+ qubit ion is paired with a 138Ba+ coolant ion.

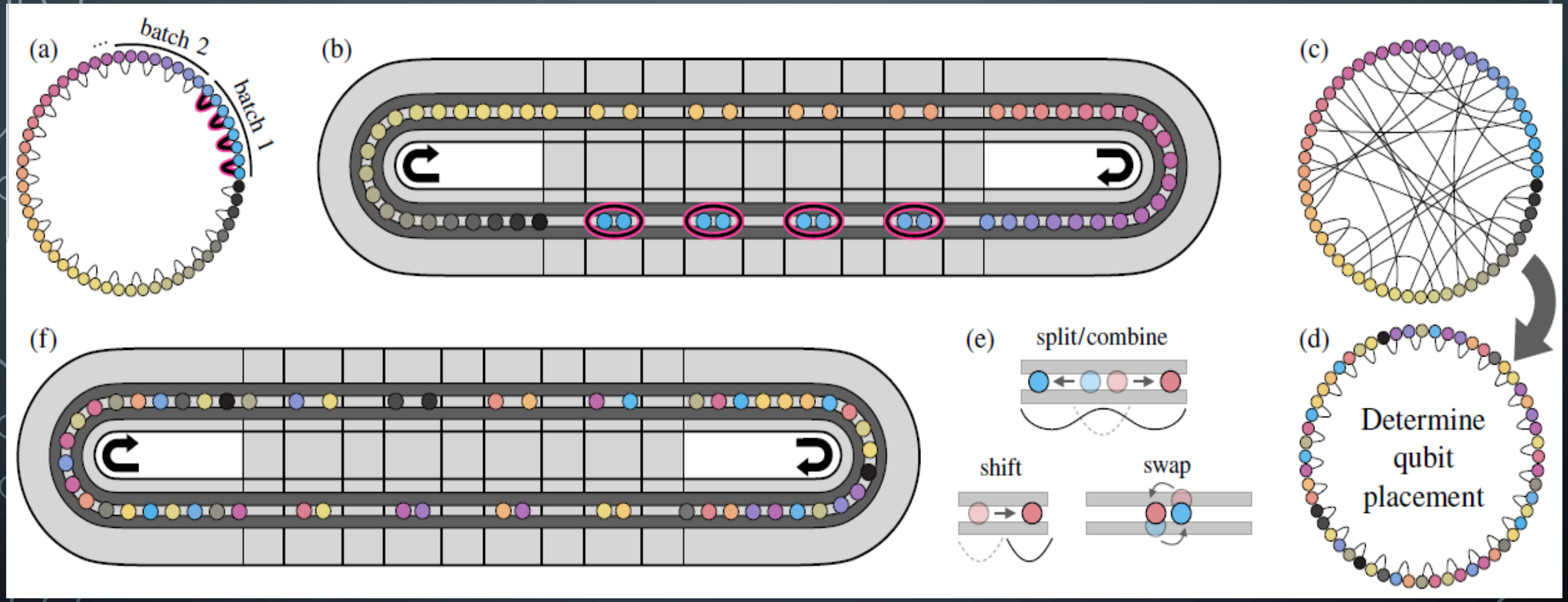

Fig. 1. Race track-shaped surface-electrode trap (p.2)

KEY THEMES:

- Random quantum circuits
- Classic Simulation
- Quantum computing
- Gate fidelity
- Advantage

NOTEBOOkLM-Google

GLOSSARY OF KEY TERMS

NOTEBOOkLM-Google

- Quantum Random Circuit (RCS): A quantum circuit composed of randomly chosen gates from a specific set of gates.
- H2 Quantum Computer: A trapped-ion quantum computer developed by Quantinuum.
- Complexity Density: A metric that quantifies the fraction of qubits that contribute to the difficulty of simulating a circuit.
- Circuit Geometry: A pattern of connectivity between qubits in a quantum circuit.
- Mirror Benchmarking: A technique for estimating the fidelity of a quantum circuit by running the circuit followed by its inverse.
- Linear Cross Entropy (FXEB): A metric for evaluating fidelity in RCS experiments by comparing the probability distribution of measured bitstrings with the ideal distribution.

GLOSSARY OF KEY TERMS

- Memory Error: Decoherence or errors introduced during the transport of ions in a quantum computer of trapped ions.
- Density Matrix Renormalization Group (DMRG): An algorithm for approximating the ground state of a many-body quantum system and simulating the evolution of quantum circuits.
- Bond Dimensionality: A parameter that controls the amount of entanglement that an MPS representation of a quantum state can capture.
- 2Q Entanglement Gate: Quantum gate that generates entanglement between two qubits.
- Quantum Advantage: The ability of a quantum computer to perform a task that is untreatable by classical computers.

NOTEBOOkLM-Google

GLOSSARY OF KEY TERMS

- Ytterbium (Yb) is used in quantum computing for its stable electronic transitions, low decoherence, and laser cooling capability, which improves the accuracy of quantum gates.
- What about the 2D and RCS explanation? 2D: This refers to quantum circuits in a two-dimensional structure, which affects the connectivity between qubits and the efficiency of classical simulations. RCS (Random Circuit Sampling): It is a method to demonstrate quantum advantage, in which random quantum circuits are executed and their results are compared with classical simulations.

NOTEBOOkLM-Google

GLOSSARY OF KEY TERMS

- Good edge expansion properties: It refers to the fact that a graph structure has good connectivity between nodes, which improves entanglement propagation and efficiency in quantum circuits.
- Sequence length: It probably refers to the number of gates or steps in a quantum circuit, which influences the fidelity and difficulty of simulation.
- Memory errors considered: Decoherence and transport errors

NOTEBOOkLM-Google

GLOSSARY OF KEY TERMS

- At shallow depth, optimal contraction does not follow this time structure, and the simulation cost can be reduced by using low-complexity quantum gates (such as UZZ(π/2) instead of iSWAP). The choice of gates affects the simulation difficulty, as some allow for more efficient decompositions and reduce computational cost.
- Do you want complexity density to tend to zero or one and why? It depends on the context. In general, if the complexity density tends to one, it means that the problem is highly complex and difficult to simulate classically. If it tends to zero, the problem is more easily solved by classical techniques.

NOTEBOOkLM-Google

WHAT IS THE H2 QUANTUM COMPUTER AND HOW IS IT DIFFERENT FROM OTHER QUANTUM COMPUTERS?

The H2 is a quantum computer from Quantinuum based on the "Charge-Coupled Quantum Computer" (QCCD) architecture. Unlike other architectures, the H2's QCCD allows for arbitrary connectivity between its qubits, meaning that any pair of qubits can interact directly without the need for logical exchanges. This is accomplished by physically moving the trapped ions that represent the qubits inside the device.

NOTEBOOkLM-Google

HOW DO YOU RUN QUANTUM CIRCUITS WITH ARBITRARY CONNECTIVITY ON THE H2?

H2 uses a combination of "split/merge," "displacement," and "exchange" operations to move ions and place qubits that need to interact in adjacent gate zones. This process is repeated for each layer of the circuit, allowing the execution of circuits with complex interaction patterns that are not possible in architectures with limited connectivity.

NOTEBOOkLM-Google

WHAT ARE QUANTUM RANDOM CIRCUITS (RCAS) AND WHY ARE THEY IMPORTANT?

RCAs are quantum circuits where gates are chosen randomly. They are important because their classical simulation is thought to be extremely difficult for circuits deep enough and with a considerable number of qubits. This is because RCAs generate highly entangled quantum states that cannot be efficiently represented with classical methods. Thus, the successful execution of RCA on a quantum computer can demonstrate the "quantum advantage" over classical methods.

NOTEBOOkLM-Google

HOW IS THE FIDELITY OF RCAS ASSESSED IN H2?

The fidelity of RCAs in H2 is estimated by two main methods:

Mirror Benchmarking (MB): A "mirror" circuit is constructed by reversing the gates of the original RCA circuit in the middle. The probability that the final state matches the initial state (MB return probability) is used as an estimate of fidelity.

Linear cross-entropy (FXEB): The cross-entropy between the probability distribution of the results obtained in H2 and the ideal distribution of the noise-free circuit is calculated. An FXEB close to 1 indicates high fidelity.

NOTEBOOkLM-Google

WHAT ARE THE CHALLENGES TO CLASSICALLY SIMULATE RCA OF RANDOM GEOMETRIES?

The classical RCA simulation is based on the representation of the circuit as a tensor network (RT) and the contraction of this network to obtain the probability amplitude of a specific state. The difficulty of RT contraction is related to the "effective number of qubits" (Nd,N), which reflects the computational cost. For RCA with random geometries, Nd,N grows rapidly with the depth of the circuit, saturating the simulation cost of a full-state vector.

NOTEBOOkLM-Google

WHAT METHODS ARE USED TO CLASSICALLY SIMULATE RCA AND WHAT ARE ITS LIMITATIONS?

Exact contraction of RT: This method is feasible for shallow circuits, but quickly becomes unfeasible as the depth and number of qubits increases due to the exponential growth of computational cost.

MPS Simulation (DMRG): This method approximates the quantum state with a matrix product state (MPS) and evolves it over time. While it is more efficient than exact contraction, its fidelity decreases as the depth of the circuit and the amount of entanglement increases. In addition, significant computational resources are required to achieve fidelity comparable to that of H2 for deep circuits.

NOTEBOOkLM-Google

HOW DOES CHOOSING THE TWO-QUBIT GATE AFFECT THE CLASSICAL SIMULATION DIFFICULTY?

In general, two-qubit gates with a higher Schmidt range (such as iSWAP) lead to circuits that are more difficult to simulate than lower-range gates (such as UZZ). This is because higher-range gates generate more entanglement, which increases the complexity of the tensor network.

NOTEBOOkLM-Google

WHAT IMPLICATIONS DO THE H2 RESULTS HAVE FOR THE "QUANTUM ADVANTAGE"?

The H2 results demonstrate the ability of the QCCD architecture to run RCA with high fidelity and arbitrary connectivity. The difficulty of classically simulating these circuits, especially as qubit count and depth increase, suggests that H2 could achieve the "quantum advantage" in RCA execution. Importantly, however, the definitive proof of "quantum advantage" requires a thorough comparison with the best classical algorithms available.

NOTEBOOkLM-Google

WE'LL GIVE A LOOK ...

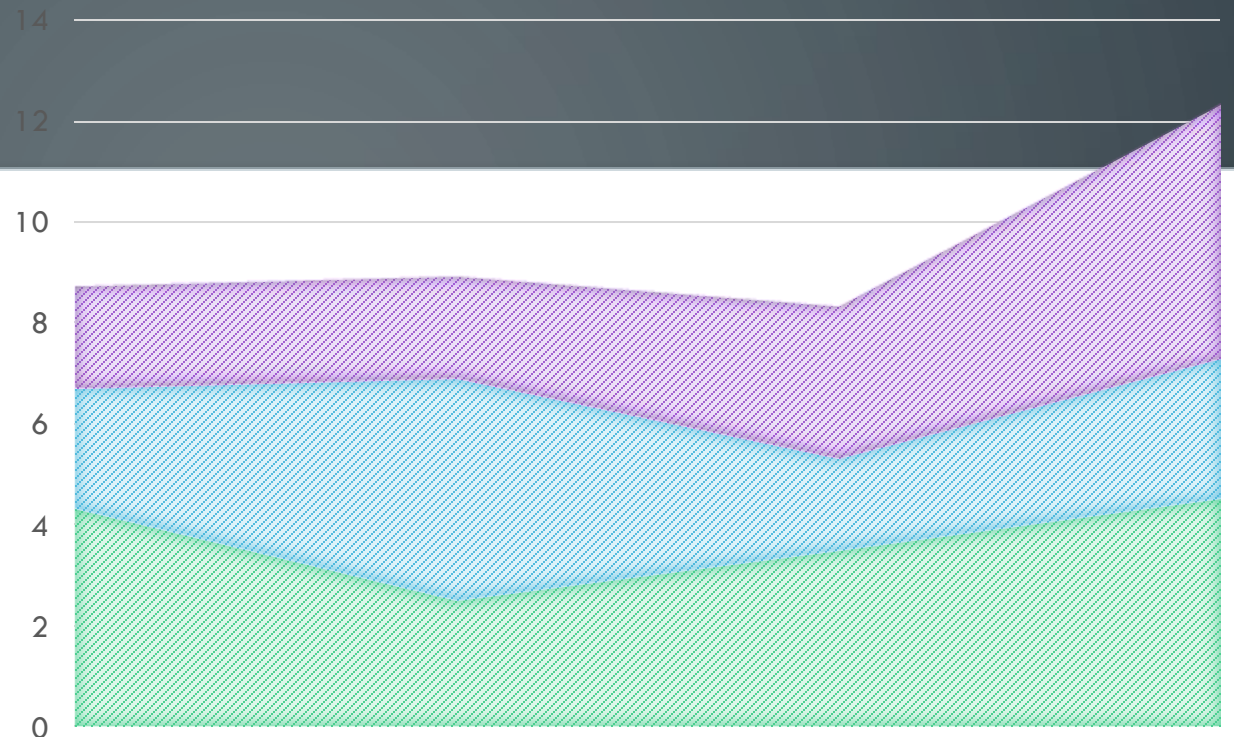

Label	Test	Value ($\times 10^{-4}$)
ϵ_{1Q}	1Q RB	0.29(4)
ϵ_{2Q}	2Q RB	15.7(5)
ϵ_{mem}	Transport 1Q RB	4.0(4)
p_{SPAM}	SPAM	14.7(9)

(DeCross et al., 2024)

AVERAGE ERROR

TABLE 1. \epsilon_{2Q} = 1.57(5)×10-3 reported in Tab. I and used to estimate circuit fidelities (p. 3)

Label	Test	Value ($\times 10^{-4}$)
ϵ_{1Q}	1Q RB	0.29(4)
ϵ_{2Q}	2Q RB	15.7(5)
ϵ_{mem}	Transport 1Q RB	4.0(4)
p_{SPAM}	SPAM	14.7(9)

FIG. 2.

“The native 2Q gate of all Quantinuum H-series hardware is the parameterized entangler $UZZ(\theta) = \exp(-i(\theta/2)Z \otimes Z)$, and each of the $(N \times d/2)$ 2Q gates is chosen to be the perfect entangler $UZZ(\pi/2)$. The 2Q gates are then sorted into d layers with N/2 gates per layer by finding a proper edge coloring of $G_{d,N}$ and then assigning one of the d colors to each of the d layers of the circuit. Edges of a given color then have their associated 2Q gates executed in the layer to which that color is assigned. A layer of Haar-random 1Q gates on every qubit is inserted immediately after qubit initialization, immediately before measurement, and between every layer of 2Q gates (for a total of d + 1 1Q layers).”

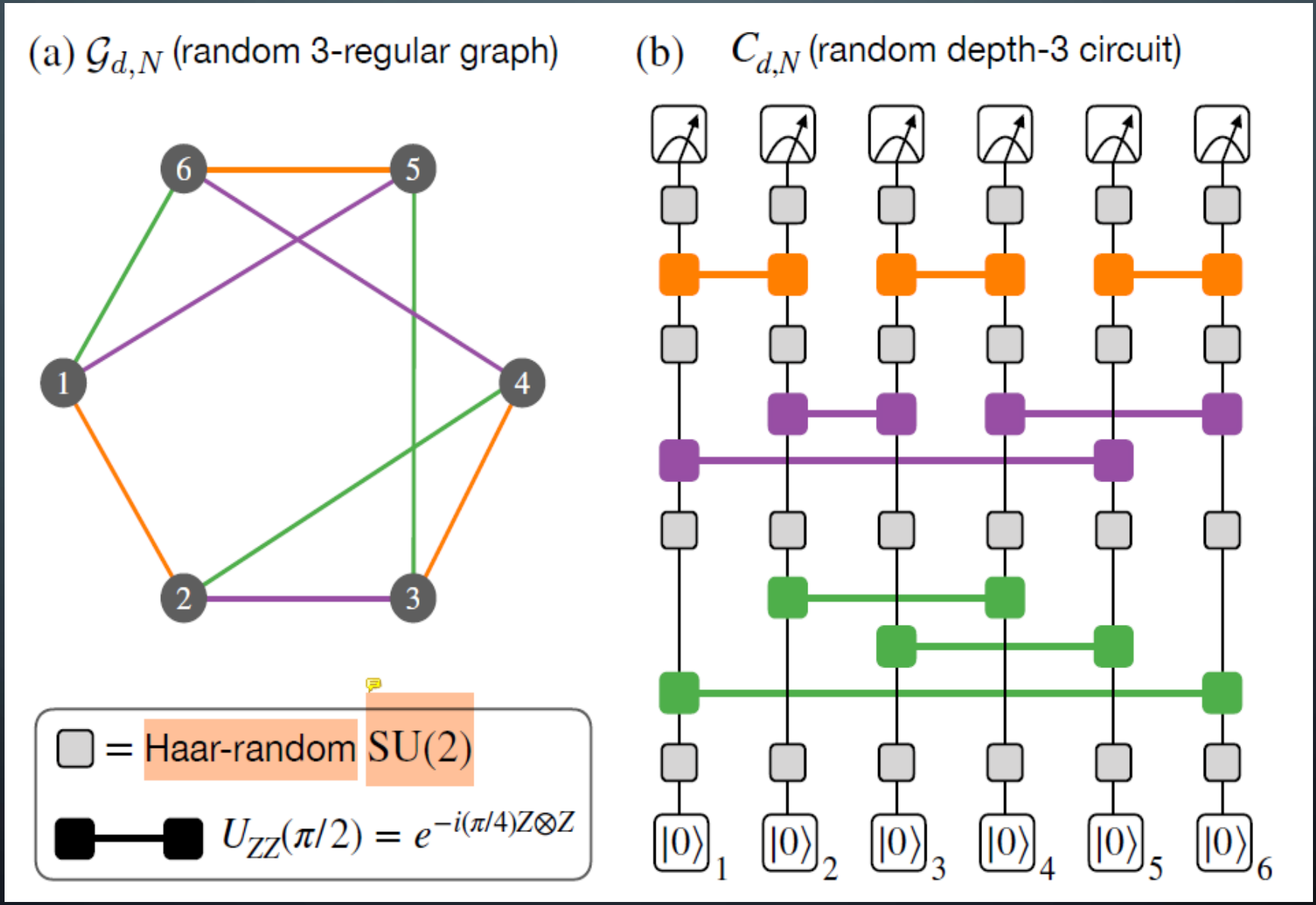
(a) $\mathcal{G}_{d,N}$ (random 3-regular graph)
6
5
1
4
2
3
= Haar-random SU(2)
$U_{ZZ}(\pi/2) = e^{-i(\pi/4)Z\otimes Z}$
(b) $C_{d,N}$ (random depth-3 circuit)
$|0\rangle_1$
$|0\rangle_2$
$|0\rangle_3$
$|0\rangle_4$
$|0\rangle_5$
$|0\rangle_6$

FIG. 3.

Comparison of complexity density Cd,N for circuits with random geometries (RG) and 2D geometries. Figures (a) and (b) show the gating pattern for a depth-4 graph on 56 qubits given random and 2D geometries, respectively. At each value (N, d), an N-node graph is assigned a coloring using either d colors (RG) or 4 colors (2D). Each circuit is comprised of layers of UZZ(π/2) gates separated by layers of random SU(2) gates on each qubit, with the UZZ gates applied to each pair of qubits whose associated vertices are joined by an edge of one color. In (a) each layer corresponds to a unique color, while in (b) the 4 colors are repeated cyclically until the desired depth is reached. Figures (c) and (d) show estimates of Cd,N for such RG and 2D circuits, respectively.

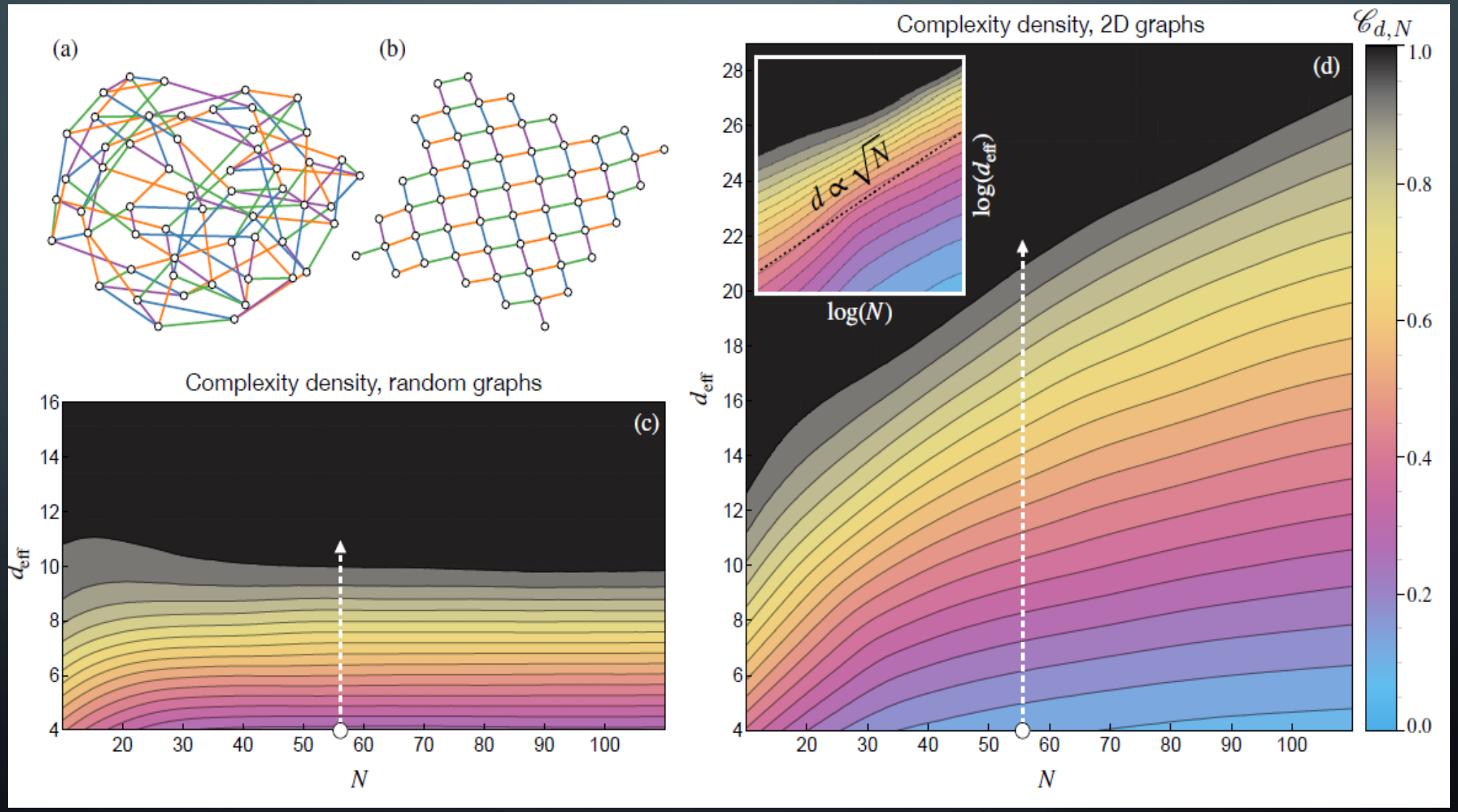
(a)
(b)
Complexity density, random graphs
(c)
d_{eff}
N
Complexity density, 2D graphs
(d)
$\mathscr{C}_{d,N}$
$d \propto \sqrt{N}$
$\log(d_{\mathrm{eff}})$
$\log(N)$

FIG. 4.

The impact of constraining memory on cost for TN contraction of a single amplitude for random quantum circuits with N = 56. (a) FLOP cost of unconstrained optimized contraction paths compared with those sliced to W=230 as a function of circuit depth, d. The cost of statevector simulation is marked for reference. (b) Size of the largest intermediate tensor, or 'contraction width', W, as a function of circuit depth. The lines represent the median behavior across 20 circuit instances, with the bands showing the min/max range.

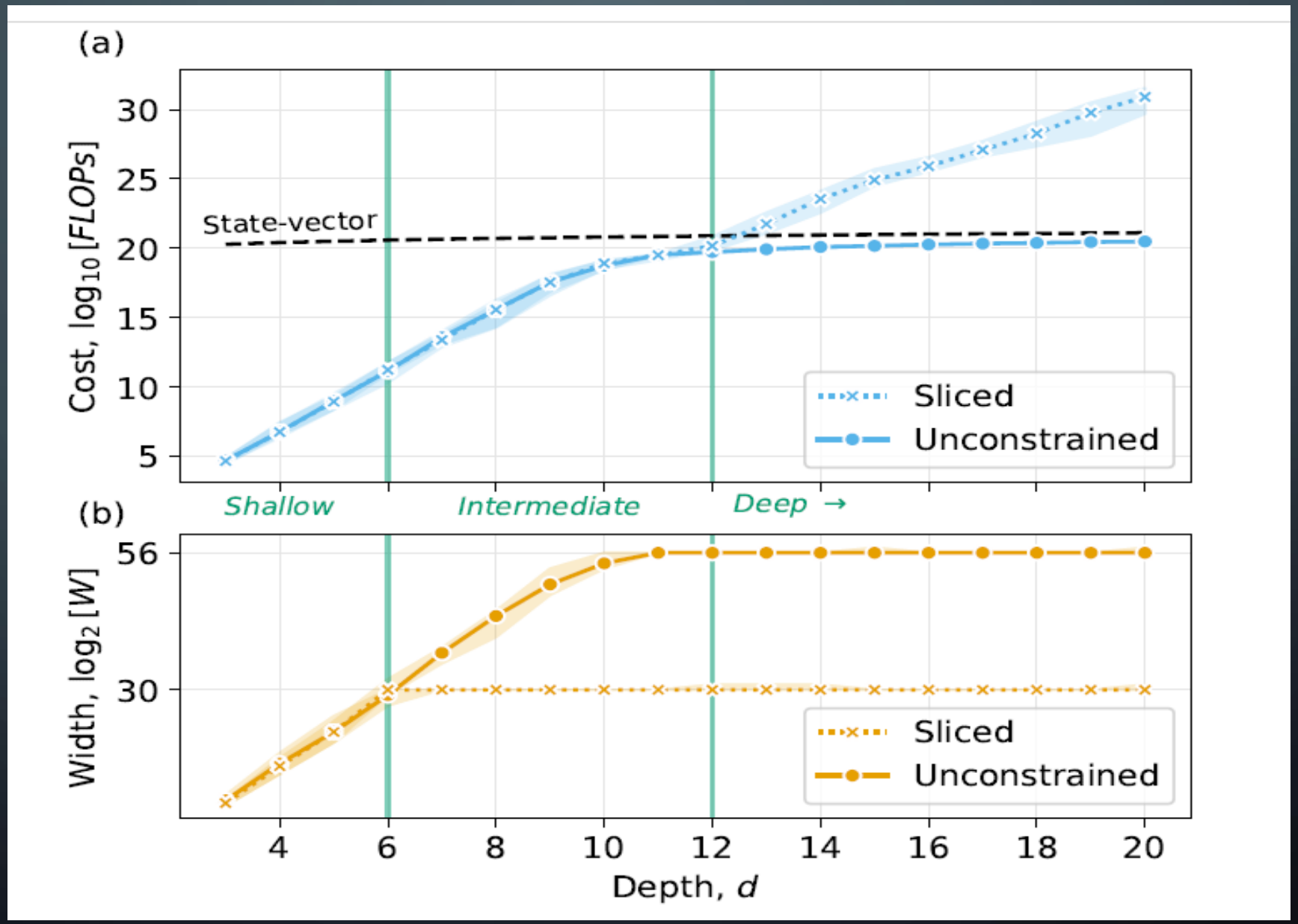
(a)
Cost, $\log_{10}[FLOPs]$
30
25
20
15
10
5
State-vector
Sliced
Unconstrained
Shallow
Intermediate
Deep →
(b)
Width, $\log_2[W]$
56
30
Sliced
Unconstrained
4
6
8
10
12
14
16
18
20
Depth, d

FIG. 5.

(a) Achievable error per gate εMPS as a function of circuit depth using DMRG for circuits with 2D and random geometries and a variety of 1Q and 2Q gate sets. All curves use a bond dimension $\chi = 256$, and shaded regions show standard deviation of the error per gate across 100 (20) circuit randomizations for random (2D) circuits. (b) Error per gate at depth 20 as a function of bond dimension. Linear extrapolation of εMPS to the experimental value of $\varepsilon \approx 3.2\times10-3$ (dotted horizontal line in this figure, see Sec. IV) from the two largest bond dimensions suggests that by depth 20, DMRG cannot simulate random geometry circuits at the fidelities achieved on H2 without employing an essentially exact representation of the full statevector (MPS bond-dimension $\chi = 2N/2=28$, green vertical line).

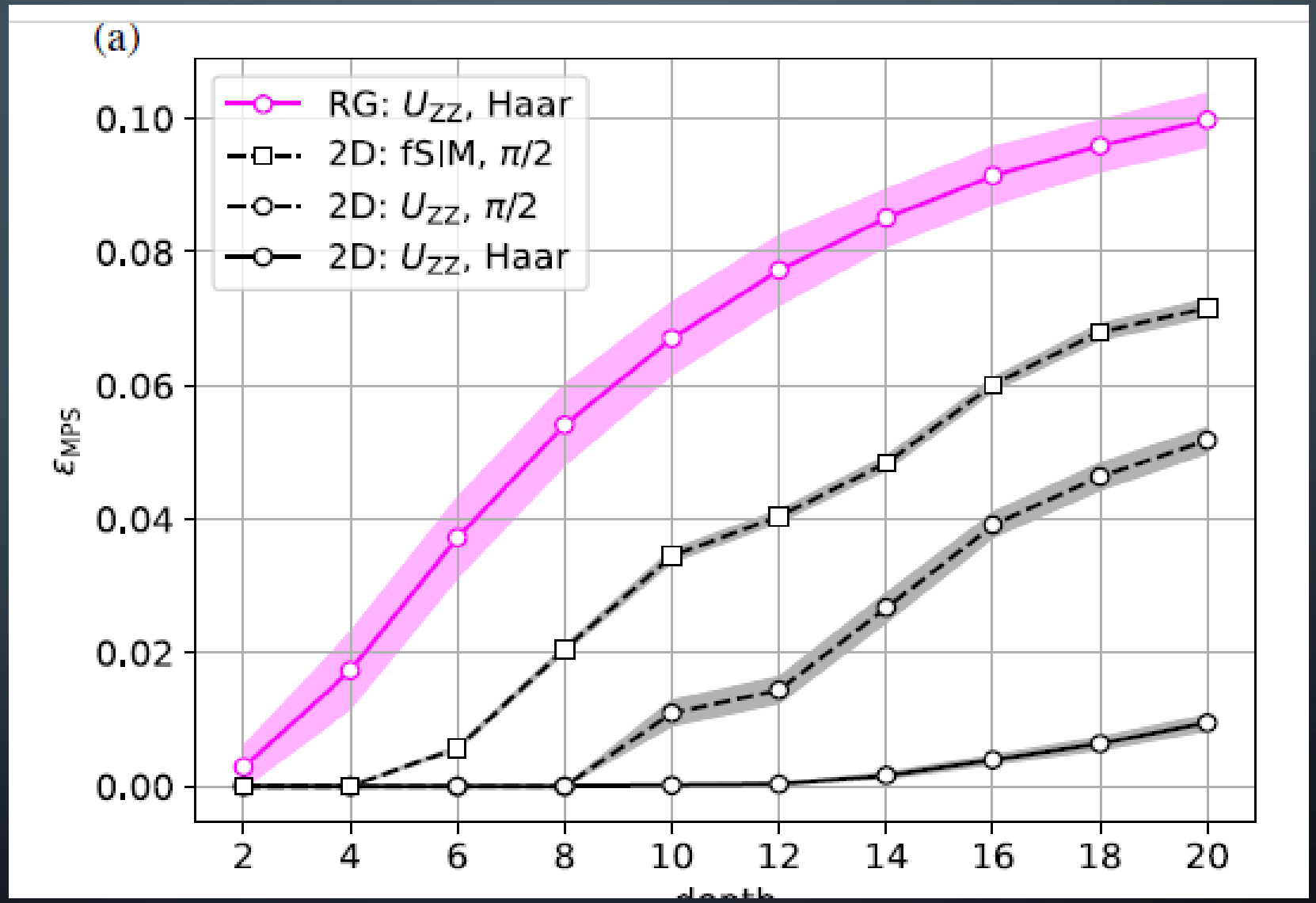
(a)
RG: U_{ZZ}, Haar
2D: fSIM, $\pi/2$
2D: U_{ZZ}, $\pi/2$
2D: U_{ZZ}, Haar
ε_{MPS}
0.00
0.02
0.04
0.06
0.08
0.10
2
4
6
8
10
12
14
16
18
20

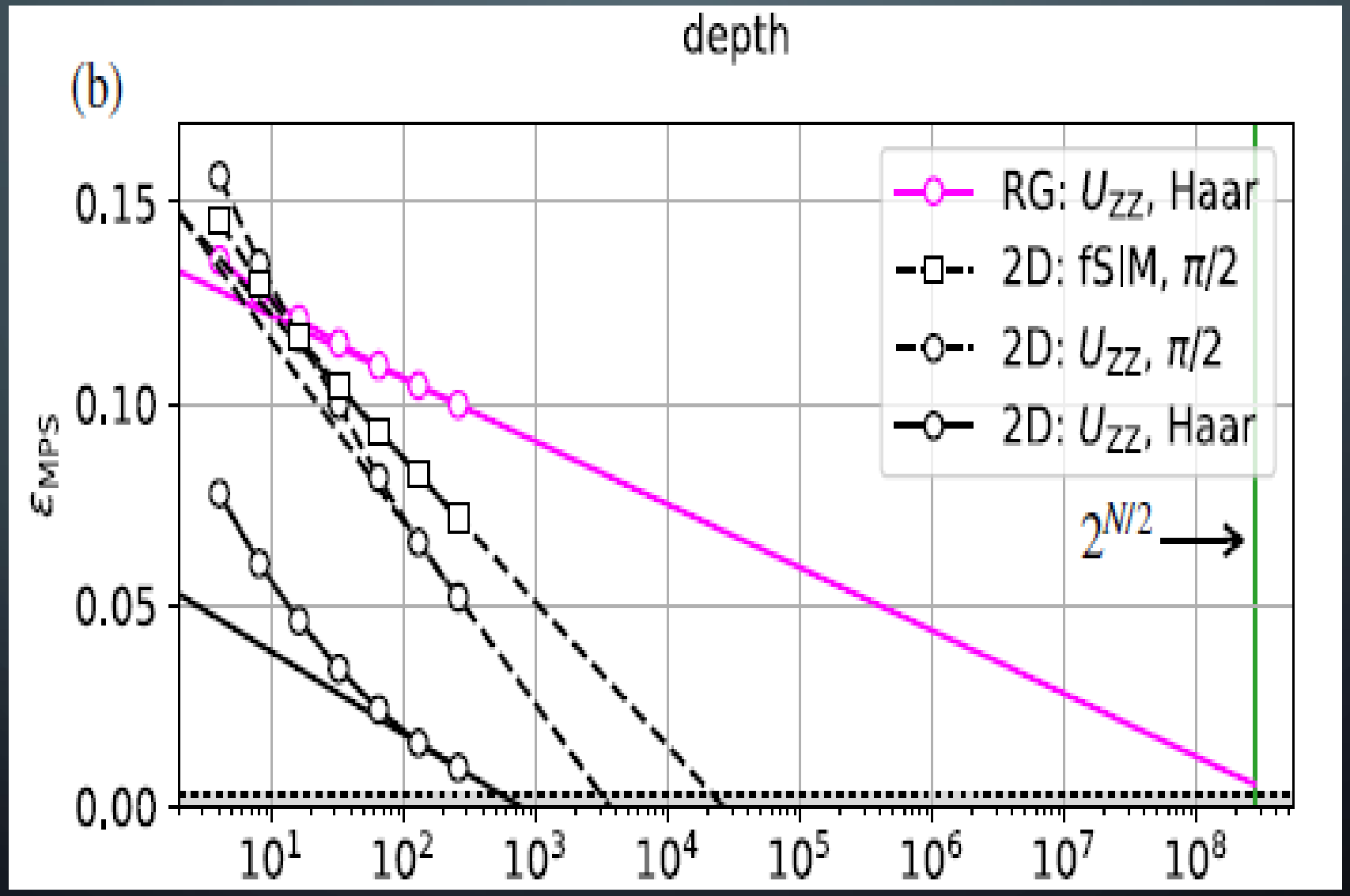
depth
(b)
0.15
0.10
0.05
0.00
ε_{MPS}
10^1
10^2
10^3
10^4
10^5
10^6
10^7
10^8
RG: U_{ZZ}, Haar
2D: fSIM, $\pi/2$
2D: U_{ZZ}, $\pi/2$
2D: U_{ZZ}, Haar
$2^{N/2}$

FIG. 6

Error per gate (ε_{MPS}) versus computational cost (in FLOPs) for both 2D and RG circuits. The results for RG (2D) circuits are again averaged over 100 (20) random circuits. All 2D circuits employ a $7\times[8]$ blocking strategy, while a variety of blocking strategies (each a different shade of pink, see main text) are attempted for the RG circuits. Cost on the x-axis is approximate, and estimates the number of floating-point operations required for DMRG using various block sizes as the MPS bond dimension is increased (including the cost of applying all gates to the MPS and all MPS overlap calculations encountered in DMRG, but not the cost of QR decompositions). (p.10)

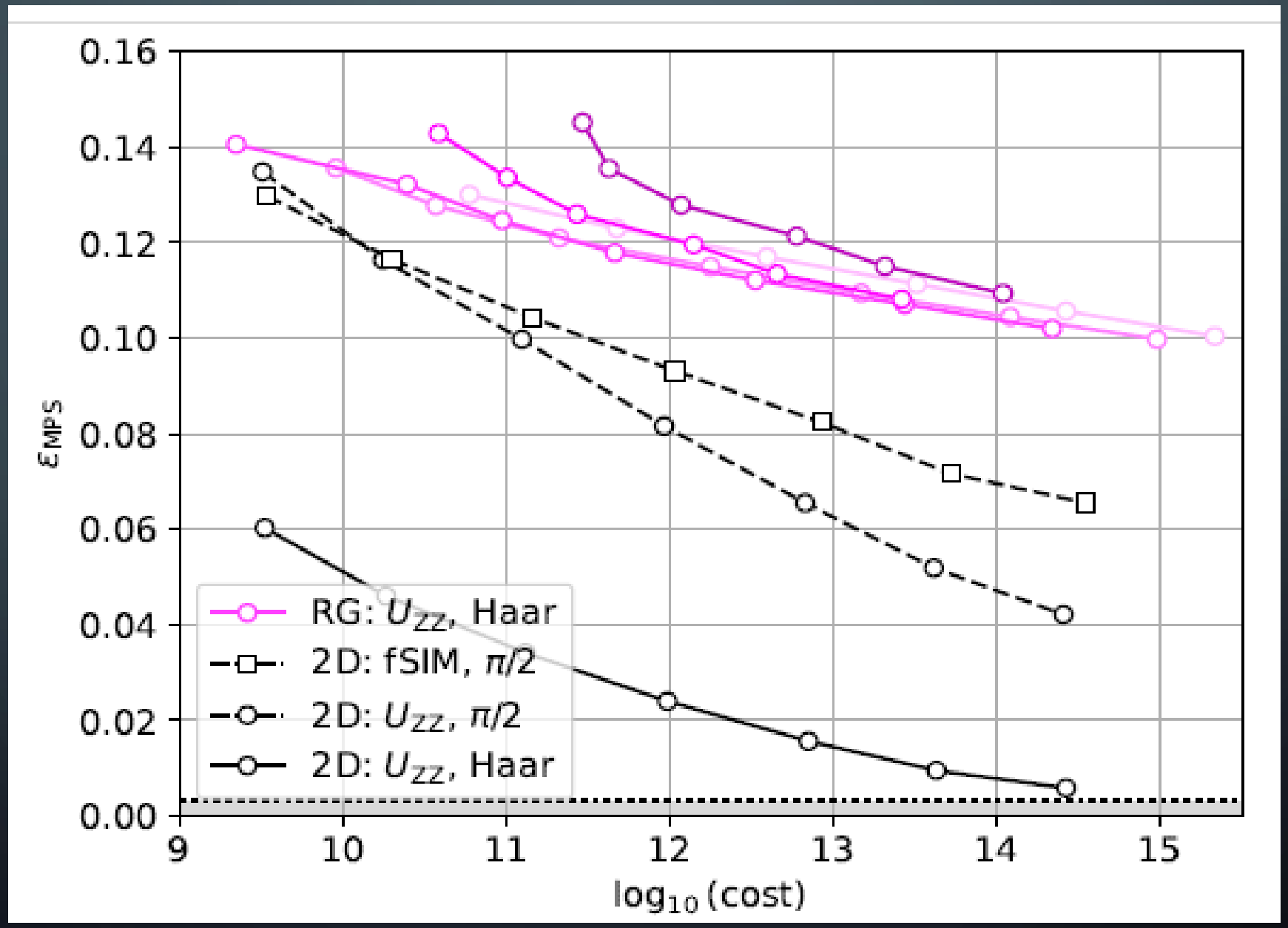
0.16
0.14
0.12
0.10
0.08
0.06
0.04
0.02
0.00
$\varepsilon_{\mathrm{MPS}}$
9
10
11
12
13
14
15
$\log_{10}$(cost)
RG: U_{ZZ}, Haar
2D: fSIM, $\pi/2$
2D: U_{ZZ}, $\pi/2$
2D: U_{ZZ}, Haar

FIG. 7.

Maximum effective qubit number Nmax achievable with 100 seconds of data as a function of the 2Q gate error rate. The black (magenta) solid curve at the bottom of each region shows results for 2D (random) geometries assuming a circuit execution time of $\tau q = 1$ s. Each progressively fainter line above the lowest corresponds to another order of- magnitude reduction in the assumed circuit time τq, with the upmost dashed line corresponding to $\tau q = 1$ μs for both geometries.

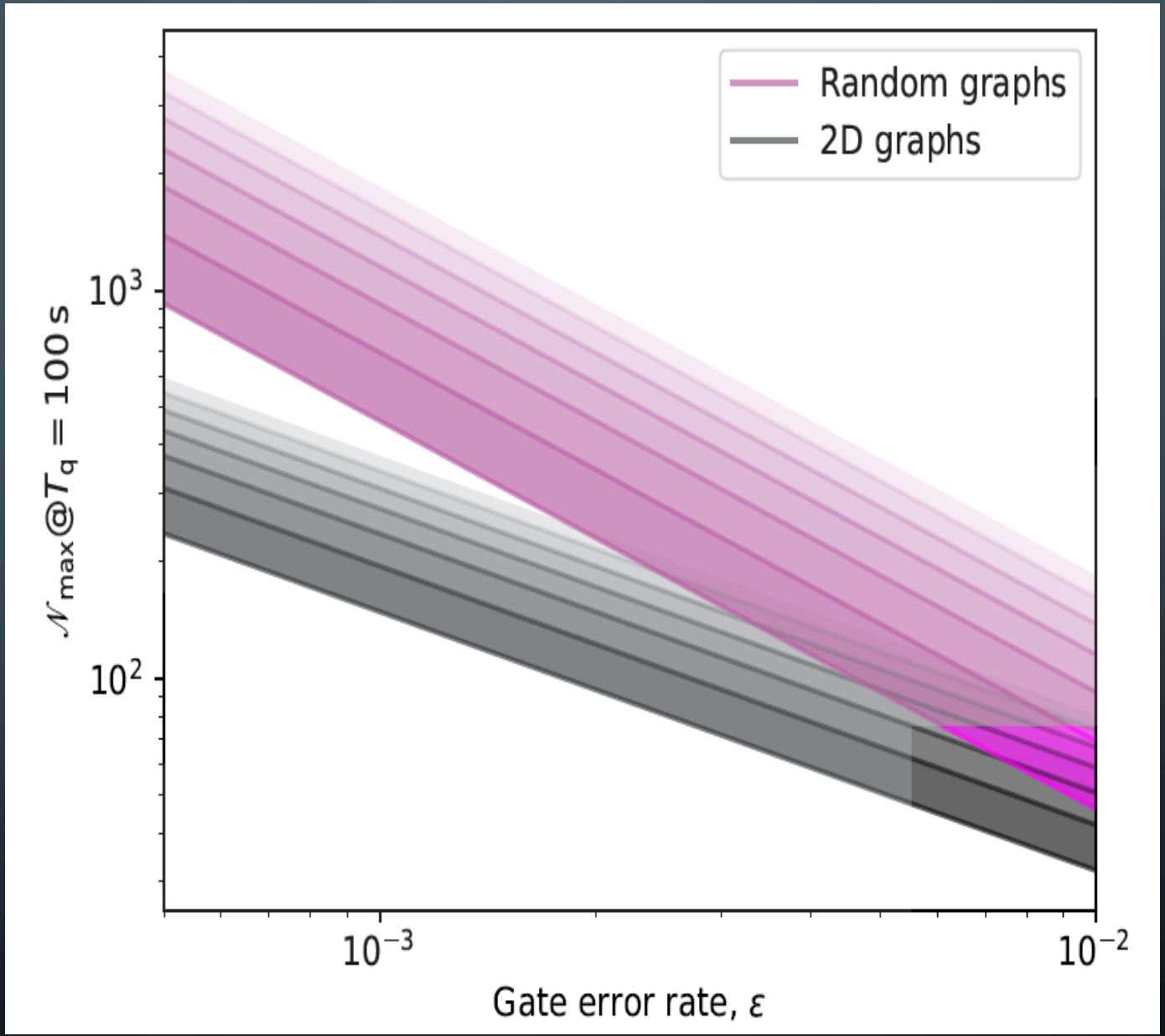
Random graphs
2D graphs
10^3
10^2
$\mathcal{N}_{\max}@T_q = 100\,s$
10^{-3}
10^{-2}
Gate error rate, ε

FIG. 8.

Illustrative examples of the circuits implemented experimentally in this paper. (a) A depth-3 RCS circuit on 6 qubits (see Fig. 2 for a description of the notation). (b) Transport 1Q RB version of the same circuit. 2Q gates with unfilled boxes denote the use of a UZZ(0) gate, which induces the same transport and cooling operations as the UZZ(π/2) but does not apply a 2Q gate. The circuit is initialized in a random bit string, in this case 011010, and the 1Q gates at the end (solid black squares) invert the cumulative action of all prior 1Q gates in order to return to this initial state, as shown in (d) for a single qubit. (c) Mirrored version of the same circuit, here initialized in the random bit string 101001. On the reversed part of the circuit all 1Q gates are inverted, UZZ(−π/2) gates are created from UZZ(π/2) gates by appending suitable 1Q Z rotations, and randomized compiling is used to twirl any potentially coherent errors in the 2Q gates into incoherent errors (avoiding any potential cancellation of coherent errors between the forward and backward halves of the circuit). All 1Q gates on the reverse half are then compiled down to the gates represented as hashed squares in (c), as shown in (e) for a single qubit.

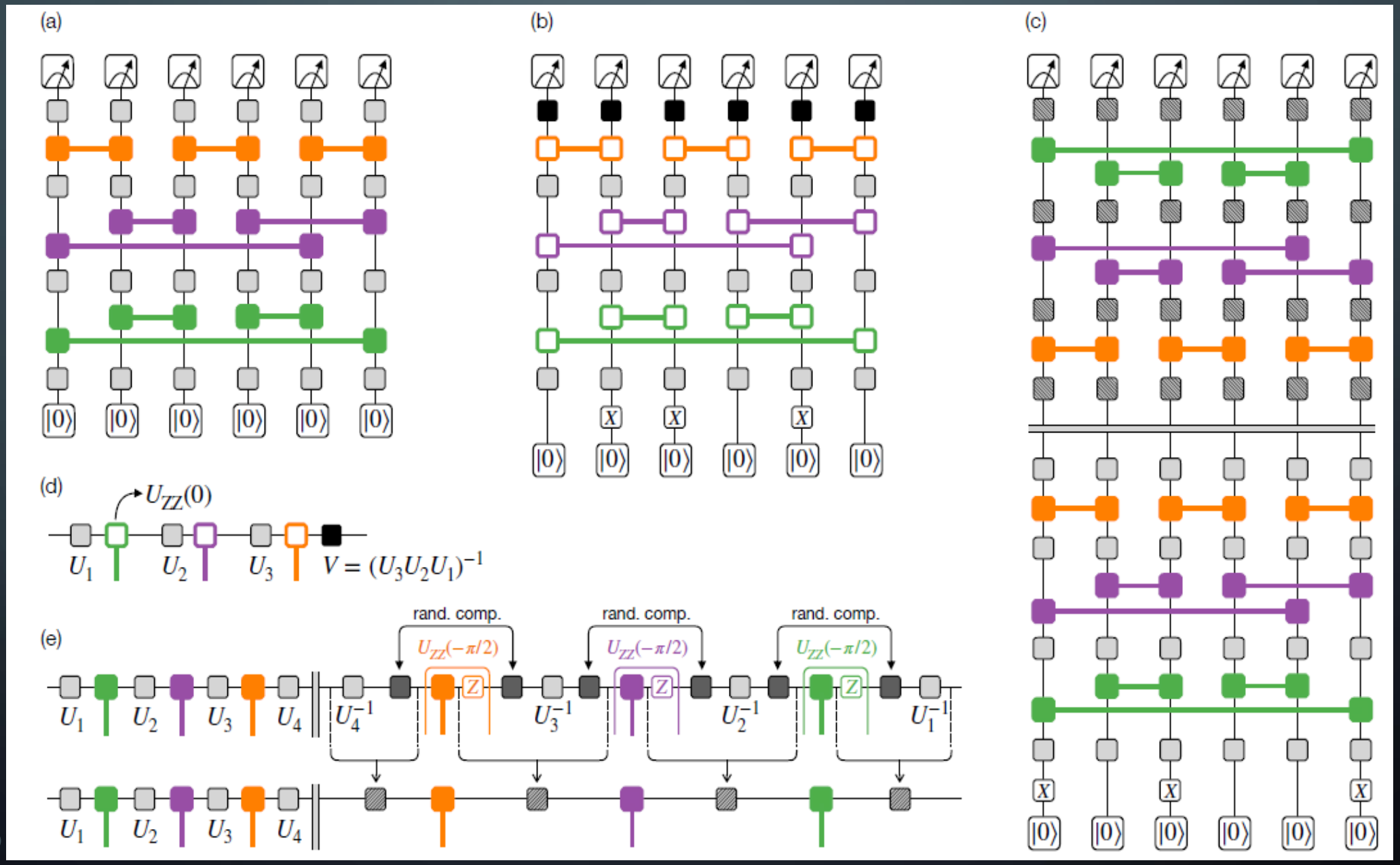
(a)
|0⟩
(b)
X
(c)
(d)
$U_{ZZ}(0)$
U_1
U_2
U_3
$V = (U_3U_2U_1)^{-1}$
(e)
rand. comp.
$U_{ZZ}(-\pi/2)$
Z
U_4
U_4^{-1}
U_3^{-1}
U_2^{-1}
U_1^{-1}

FIG. 9.

Fidelity estimation from H2 data at a variety of qubit numbers and circuit depths. (a) FMB (MB return probability, green) at N = 56 as a function of depth. We also plot a fidelity estimate at depth 12 (pink) inferred from the MB return probability at depth 24 from mirror circuits that were constructed from the exact depth-12 RCS circuits. The color gradient corresponds to the complexity density from Fig. 3. (b) FXEB (linear cross-entropy, orange) and FMB (green) as a function of qubit number N at fixed depth d = 12. (c) FXEB (orange) and FMB (green) as a function of depth at N = 40, the largest of the N we took data at that was classically verifiable with our computational resources. All uncertainties plotted represent 1σ confidence intervals on the data. The gray shaded regions represent 1σ confidence intervals on the gate-counting model arising from propagation of uncertainties on the component operation fidelities.

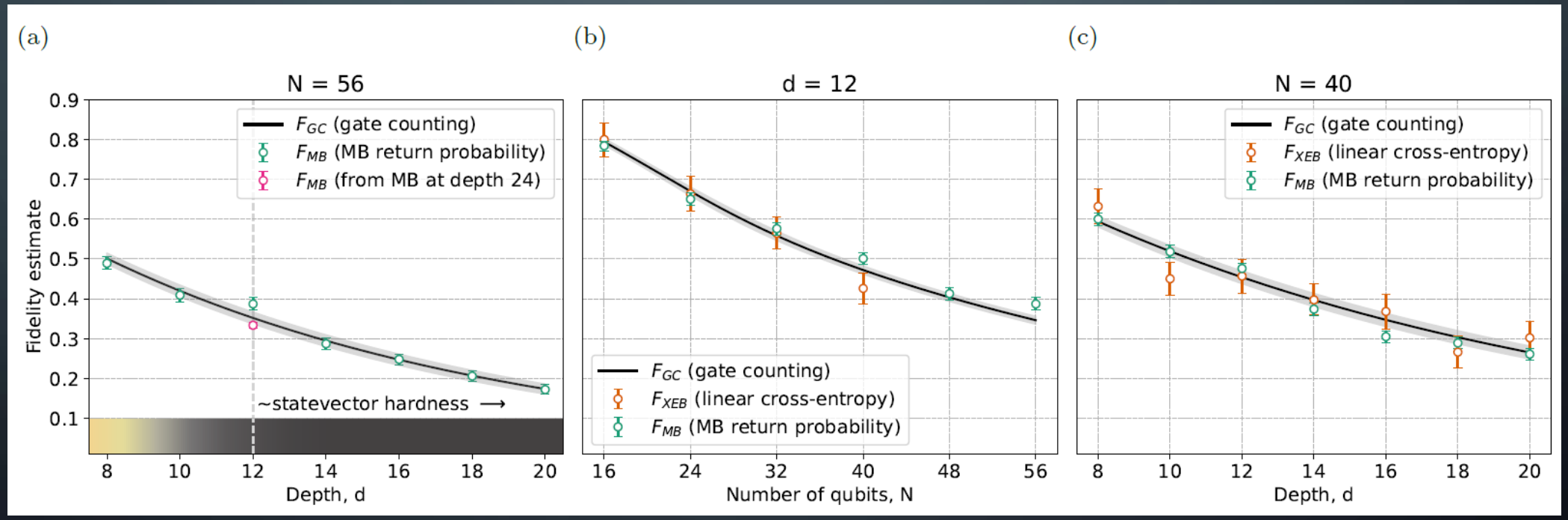
(a)
N = 56
Fidelity estimate
0.9
0.8
0.7
0.6
0.5
0.4
0.3
0.2
0.1
F_{GC} (gate counting)
F_{MB} (MB return probability)
F_{MB} (from MB at depth 24)
~statevector hardness ⟶
8
10
12
14
16
18
20
Depth, d
(b)
d = 12
F_{GC} (gate counting)
F_{XEB} (linear cross-entropy)
F_{MB} (MB return probability)
16
24
32
40
48
56
Number of qubits, N
(c)
N = 40
F_{GC} (gate counting)
F_{XEB} (linear cross-entropy)
F_{MB} (MB return probability)
8
10
12
14
16
18
20
Depth, d

¡THANKS!

IONQ

Products Company Resources Careers Blog Sign In Sign Up

NEWS IonQ Signs Historic Agreement with Toyota Tsusho Corporation to Advance Quantum Computing Opportunities in Japan ▸

Quantum is Now.

Quantum computing has the potential to change the world, and IonQ is leading the way.

Start your quantum journey

Contact a quantum solution specialist →

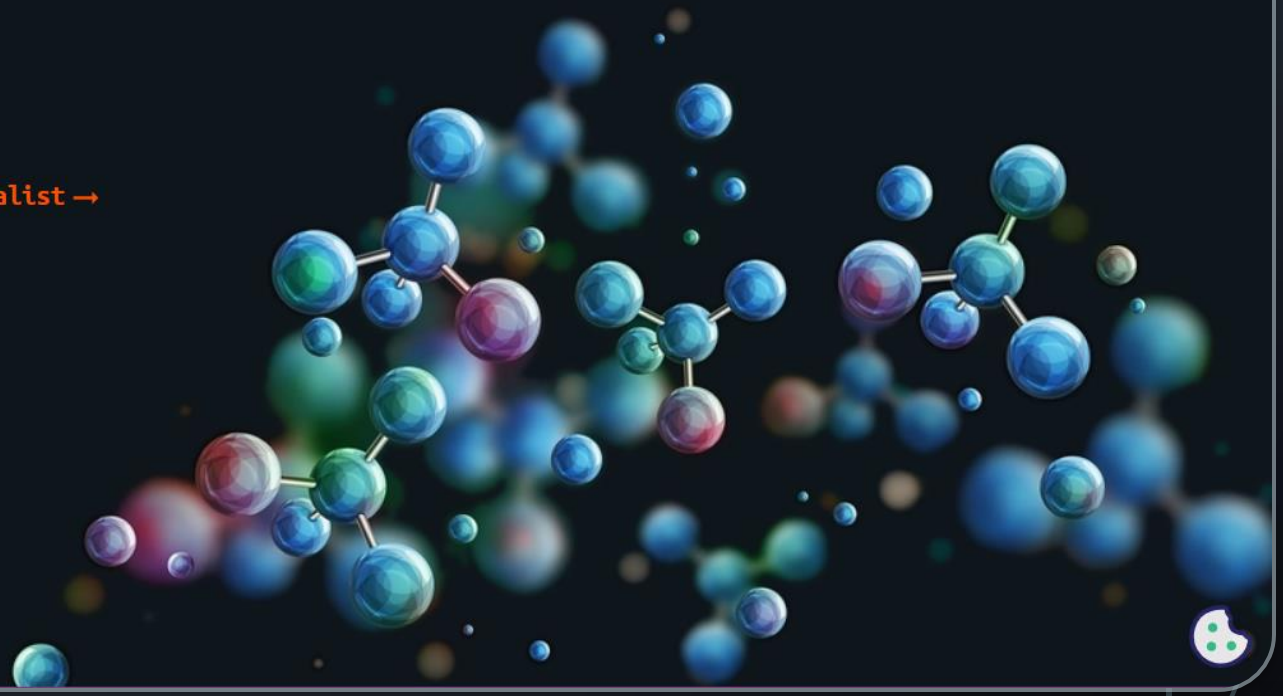

Improved drug discovery

With ~**1,000** algorithmic qubits, ⓘ we could help revolutionize the pharmaceutical industry.

Learn more about our roadmap →

IONQ

C. Monroe and J. Kim Authors Info & Affiliations. (2013). Scaling the Ion Trap Quantum Processor.

https://www.science.org/doi/10.1126/science.1231298

BIBLIOGRAPHY

[1]. Pino, J. M., Dreiling, J. M., Figgatt, C., Gaebler, J. P., Moses, S. A., Allman, M. S., Baldwin, C. H., Foss-Feig, M., Hayes, D., Mayer, K., Ryan-Anderson, C., & Neyenhuis, B. (2020). Demonstration of the trapped-ion quantum-CCD computer architecture. https://doi.org/10.1038/s41586-021-03318-4

[2]. Moses, S. A., Baldwin, C. H., Allman, M. S., Ancona, R., Ascarrunz, L., Barnes, C., Bartolotta, J., Bjork, B., Blanchard, P., Bohn, M., Bohnet, J. G., Brown, N. C., Burdick, N. Q., Burton, W. C., Campbell, S. L., Campora, J. P., Carron, C., Chambers, J., Chan, J. W., … Pino, J. M. (2023). A Race-Track Trapped-Ion Quantum Processor. Physical Review X, 13(4). https://doi.org/10.1103/PhysRevX.13.041052

[3]. DeCross, M., Haghshenas, R., Liu, M., Rinaldi, E., Gray, J., Alexeev, Y., Baldwin, C. H., Bartolotta, J. P., Bohn, M., Chertkov, E., Cline, J., Colina, J., DelVento, D., Dreiling, J. M., Foltz, C., Gaebler, J. P., Gatterman, T. M., Gilbreth, C. N., Giles, J., … Foss-Feig, M. (2024). The computational power of random quantum circuits in arbitrary geometries. http://arxiv.org/abs/2406.02501

[4]. C. Monroe and J. Kim. (2013). Scaling the Ion Trap Quantum Processor. Vol 339, Issue 6124. pp. 1164-1169. DOI: 10.1126/science.1231298https://www.science.org/doi/10.1126/science.1231298

CIBERGRAPHY

NOTEBOOkLM: https://notebooklm.google.com/notebook/2954d414-105c-40b3-8933-ba1854917f5a?_gl=1*k4fmwy*_ga*MTMzMjUxMDYxLjE3MzMzNjgxNjU.*_ga_W0LDH41ZCB*MTczMzM2ODE2NS4xLjAuMTczMzM2ODE2NS42MC4wLjA.&original_referer=https:%2F%2Fnotebooklm.google%23&pli=1

RECOMMENDED!! :

[5]. Grzesiak et al., 2020. Efficient arbitrary simultaneously entangling gates on a trapped-ion quantum computer. Nature Communications. https://www.nature.com/articles/s41467-020-16790-9

[6]. Wan et al., 2019. Quantum gate teleportation between separated qubits in a trapped-ion processor. Science, Volume 364 | Issue 6443 https://www.science.org/doi/epdf/10.1126/science.aaw9415